


Communication

Highly Efficient Solution-Processed Bluish-Green Thermally Activated Delayed Fluorescence Compounds Using Di(pyridin-3-yl)methanone as Acceptor

Yuting He ¹, Cheng Zhang ², Hao Yan ³, Yongshuai Chai ⁴ and Deyun Zhou ^{1,*} 

¹ School of Microelectronics, Northwestern Polytechnical University, Xi'an 710129, China; heyt@nwpu.edu.cn

² Key Laboratory of Functional Textile Material and Product, Ministry of Education, School of Textile Science and Engineering, Xi'an Polytechnic University, Xi'an 710048, China; zhangcheng@xpu.edu.cn

³ School of Advanced Materials, Peking University Shenzhen Graduate School, Peking University, Shenzhen 518055, China; yanhao@pku.edu.cn

⁴ Interdisciplinary Research Center on Biology and Chemistry, Shanghai Institute of Organic Chemistry, Chinese Academy of Sciences, Shanghai 201210, China; chaisy@sioc.ac.cn

* Correspondence: dyzhounpu@nwpu.edu.cn

Abstract: Solution-processed devices with thermally activated delayed fluorescence (TADF) compounds have gained great attention due to their low cost and high performance. Here, two solution-processable TADF emitters named ACCz-DPyM and POxCz-DPyM were synthesized by coupled 9,10-dihydro-9,9-dimethylacridine or phenoxazine modified carbazole as donor with di(pyridin-3-yl)methanone as acceptor. Both TADF compounds show same small ΔE_{ST} of 0.04 eV and high PLQY of 66.2% and 58.2%. The devices fabricated by ACCz-DPyM and POxCz-DPyM as emitters show excellent performance as solution-processed with low turn-on voltage of 4.0 and 3.4 V, high luminance of 6209 and 3248 cd m⁻² at 8 V, the maximum current efficiency of 9.9 and 15.9 cd A⁻¹, the maximum external quantum efficiency of 6.6% and 6.5% and low efficiency roll-off. The solution-processed device based on ACCz-DPyM shows bluish-green emission. These results show that ACCz-DPyM and POxCz-DPyM are suitable for solution processing devices.

Keywords: TADF; solution-processed; OLED



Citation: He, Y.; Zhang, C.; Yan, H.; Chai, Y.; Zhou, D. Highly Efficient Solution-Processed Bluish-Green Thermally Activated Delayed Fluorescence Compounds Using Di(pyridin-3-yl)methanone as Acceptor. *Photonics* **2023**, *10*, 456. <https://doi.org/10.3390/photronics10040456>

Received: 14 February 2023

Revised: 12 April 2023

Accepted: 13 April 2023

Published: 14 April 2023



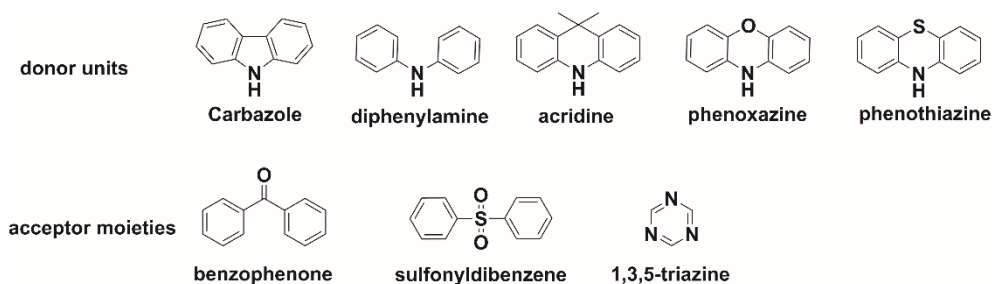
Copyright: © 2023 by the authors. Licensee MDPI, Basel, Switzerland. This article is an open access article distributed under the terms and conditions of the Creative Commons Attribution (CC BY) license (<https://creativecommons.org/licenses/by/4.0/>).

1. Introduction

Thermally activated delayed fluorescence (TADF) materials have attracted considerable interest from researchers over the past few years due to their ability to utilise triplet state excitons through rapid reverse intersystem crossing (RISC) processes from an excited triplet state (T_1) to a singlet state (S_1), theoretically enabling 100% internal quantum electrons (IQE) [1–8]. Most high-performance TADF-based organic light-emitting diodes (OLEDs) are manufactured by a vacuum deposition process [9–14], which requires a complex manufacturing process and is costly. However, a truly low-cost OLED device could be developed by solution processing [15–18]. In recent investigations, the performance of solution processing devices has also been further developed [19–23], while it is still to be improved compared with that of the vacuum evaporation device at present.

Generally, TADF molecules are mainly concentrated on a twisted donor (D)-acceptor (A) backbone, which can effectively separate the highest occupied molecular orbital (HOMO) from the lowest unoccupied molecular orbital (LUMO) spatially, resulting in a small ΔE_{ST} [24–29]. As shown in Scheme 1, carbazole, diphenylamine, acridine, phenoxazine and phenothiazine are usually selected as donor units, while benzophenone, sulfonyldibenzene and 1,3,5-triazine are usually regarded as acceptor moieties [30–33]. However, the construction of TADF molecules with a D-A backbone using acridine or phenoxazine-modified carbazole as the donor unit and di(pyridin-3-yl)methanone as the acceptor unit is hardly reported. Moreover, increasing molecular weight can effectively

improve the solution processability of TADF materials [31,34]. Hence, in order to obtain suitable solution-processed TADF materials, we designed and synthesized two TADF compounds named ACCz-DPyM and POxCz-DPyM which comprised a central di(pyridin-3-yl)methanone (DPyM) acceptor core coupled with 3,6-bis(9,9-dimethylacridin-10(9H)-yl)-9H-carbazole (ACCz) and 3,6-di(10H-phenoxazin-10-yl)-9H-carbazole (POxCz) as donors. ACCz-DPyM and POxCz-DPyM have a higher molecular weight than the small molecule TADF emitters. The major difference in molecular structure between the two emitters is the 9,10-dihydro-9,9-dimethylacridine of ACCz-DPyM and the phenoxazine of POxCz-DPyM on POxCz. The absence of such a heteroatom in 9,10-dihydro-9,9-dimethylacridine, in contrast to the presence of an oxygen atom in phenolizine, may make the structure of ACCz more molecularly rigid than POxCz. The phenoxazine has stronger electron-donating ability than acridine. Therefore, it could be predicted that the emission spectrum of POxCz-DPyM will be red-shifted compared to ACCz-DPyM. The PL quantum yields (PLQY) of ACCz-DPyM and POxCz-DPyM were 66.2% and 58.2% in film state, respectively. The ACCz-DPyM-based and POxCz-DPyM-based solution-processed devices exhibited the maximum electroluminescence (EL_{max}) of 510 vs. 560 nm, the maximum current efficiency (CE_{max}) of 9.9 vs. 15.9 $cd A^{-1}$, the maximum external quantum efficiency (EQE_{max}) of 6.6% vs. 6.5%, the maximum luminance (L_{max}) of 6209 vs. 3248 $cd m^{-2}$ at 8 V and CIE coordinates of (0.28, 0.48) and (0.43, 0.51) with relatively low turn-on voltage of 4.0 vs. 3.4 V, respectively. Furthermore, both solution-processed devices have shown low efficiency roll-off.



Scheme 1. The structure of donor and acceptor units.

2. Results and Discussion

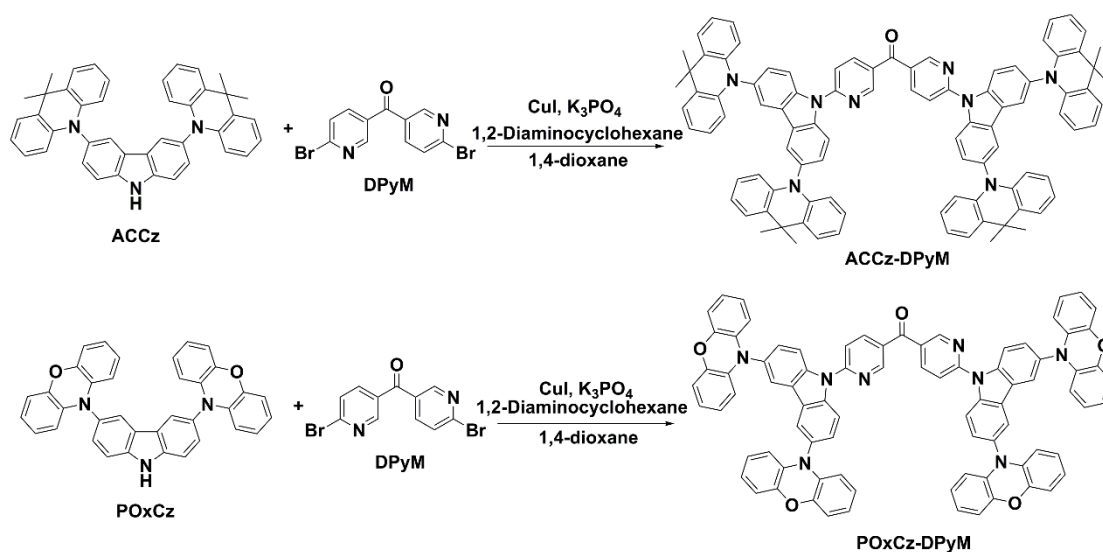
2.1. Synthesis and Characterization

The synthetic lines and molecule structures of the ACCz-DPyM and POxCz-DPyM are illustrated in Scheme 2. The TADF compounds had been successfully synthesized according to the literature methods [35]. The molecule structure of the compounds was determined by 1H NMR, ^{13}C NMR and HRMS.

2.2. Thermal Stability and Film-Forming Properties of ACCz-DPyM and POxCz-DPyM

The thermal gravimetric analyses (TGA) and differential scanning calorimetry (DSC) are tested to research the thermal properties of ACCz-DPyM and POxCz-DPyM. As shown in Figure S1, TGA show that both of these materials have high thermal decomposition temperatures with 434 °C and 527 °C for ACCz-DPyM and POxCz-DPyM, respectively. The DSCs show that the glass transition temperature (T_g) of ACCz-DPyM and POxCz-DPyM are 254 °C and 168 °C, respectively. The results of thermal analysis show that ACCz-DPyM and POxCz-DPyM have good thermal stability, which may attribute to bulky structure. The high thermal stabilities of ACCz-DPyM and POxCz-DPyM contribute to the formation of amorphous films through solution processing. Additionally, in order to research morphology further, it is necessary to investigate the surface morphologies of thin film of the two emitters, which are analysed by atomic force microscopy (AFM), which is shown in Figure S2. The films of ACCz-DPyM and POxCz-DPyM show pinhole-free morphologies, with root mean squares (RMSs) of 0.50 and 0.64 nm. It can be concluded that the bulky structure of the two emitters is beneficial for improving the morphological

stability of the films, which is important for the fabrication of highly electronic sol-gel treated OLEDs.



Scheme 2. Synthetic route for the compounds ACCz-DPyM and POxCz-DPyM.

2.3. Electrochemical Properties and Theoretical Calculation

Figure S3 shows cyclic voltammetry (CV) of ACCz-DPyM and POxCz-DPyM. ACCz-DPyM and POxCz-DPyM exhibited quasi-reversible oxidation processes. The oxidation potentials of ACCz-DPyM and POxCz-DPyM are 0.18 and 0.28 V, respectively. According to the equation $\text{HOMO} = -(4.8 + E_{\text{ons}}^{\text{ox}})$, the energy levels corresponding to the HOMO of ACCz-DPyM and POxCz-DPyM are estimated to be -4.98 and -5.08 eV, respectively. The LUMO energy levels of ACCz-DPyM and POxCz-DPyM estimated from the HOMO energy levels and optical bandgaps were -2.20 and -2.51 eV. Additionally, in order to research the structure-property relationships of the compounds, DFT calculations were used to calculate HOMO and LUMO distributions of ACCz-DPyM and POxCz-DPyM. As shown in Figure 1, the HOMO distributions of both emitters are located at the donors, and LUMOs are located at the acceptors, respectively. The HOMO and LUMO distributions of the two target molecules are well separated, which leads to a small ΔE_{ST} . The calculated HOMO levels of ACCz-DPyM and POxCz-DPyM were -4.95 and -4.72 eV, while the calculated LUMO levels were -2.45 and -2.53 eV for ACCz-DPyM and POxCz-DPyM, respectively; the results of DFT calculation are comparable with experimental data.

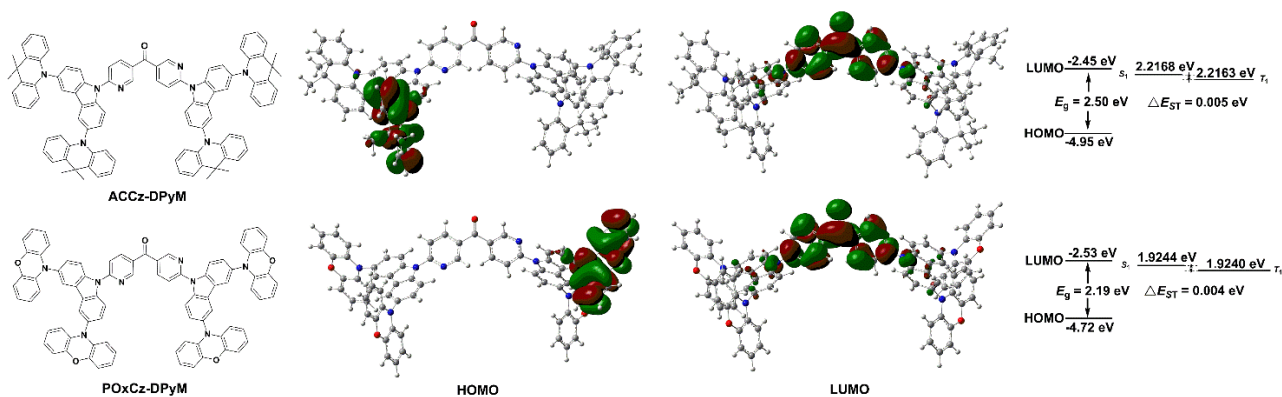


Figure 1. Optimized molecular orbital based on B3LYP/6-31G*, HOMO and LUMO energy levels for two compounds.

2.4. Photophysical Properties

The UV-visible absorption spectra and photoluminescence (PL) spectra of the target compounds ACCz-DPyM and POxCz-DPyM in dilute solution are shown in Figure 2a, and the data are summarized in Table 1. For the target molecule ACCz-DPyM, the absorption band of 330–450 nm is attributed to intramolecular charge transfer (ICT) transitions between the ACCz moieties as donor and the DPyM unit as acceptor, with the high energy absorption coming from local transitions between the ACCz and DPyM units, while for POxCz-DPyM, the absorption band of 305–500 nm is attributed to ICT and local transitions between the POxCz and DPyM units in dilute solution [29,30]. It is well known that the fundamental principles of TADF molecules are the separation of HOMO–LUMO and the small enough ΔE_{ST} value [1]. The experimental ΔE_{ST} of two emitters doped in the mCBP as host material (8 wt%) were determined by the onsets of the fluorescence and phosphorescence spectra at 77 K (delayed 100 μ s) (Figure 2b), which were both estimated to 0.04 eV for ACCz-DPyM and POxCz-DPyM. Moreover, Figure 1 shows that the HOMO orbitals of the target molecules ACCz-DPyM and POxCz-DPyM are all located on the ACCz or POxCz moieties without distribution on the acceptor moiety. In contrast, the LUMO orbitals of the target compounds ACCz-DPyM and POxCz-DPyM are located almost on the DPyM unit, with a slight distribution on the donor unit. Hence, the spatial separation of the HOMO and LUMO between the donor and acceptor units in ACCz-DPyM and POxCz-DPyM are beneficial to realize a small ΔE_{ST} . The theoretical calculations values of ΔE_{ST} were 0.005 and 0.004 eV for ACCz-DPyM and POxCz-DPyM, respectively. As shown in Figure 3, the transient PL decay experiment of the two doped films shows prompt fluorescence lifetimes of 39.8 ns and 98.9 ns and delayed fluorescence lifetimes of 7.2 μ s and 8.7 μ s, respectively. The absolute PL quantum efficiency values measured using an integrating sphere for the two doped films are 66.2% and 58.2% for ACCz-DPyM and POxCz-DPyM, respectively.

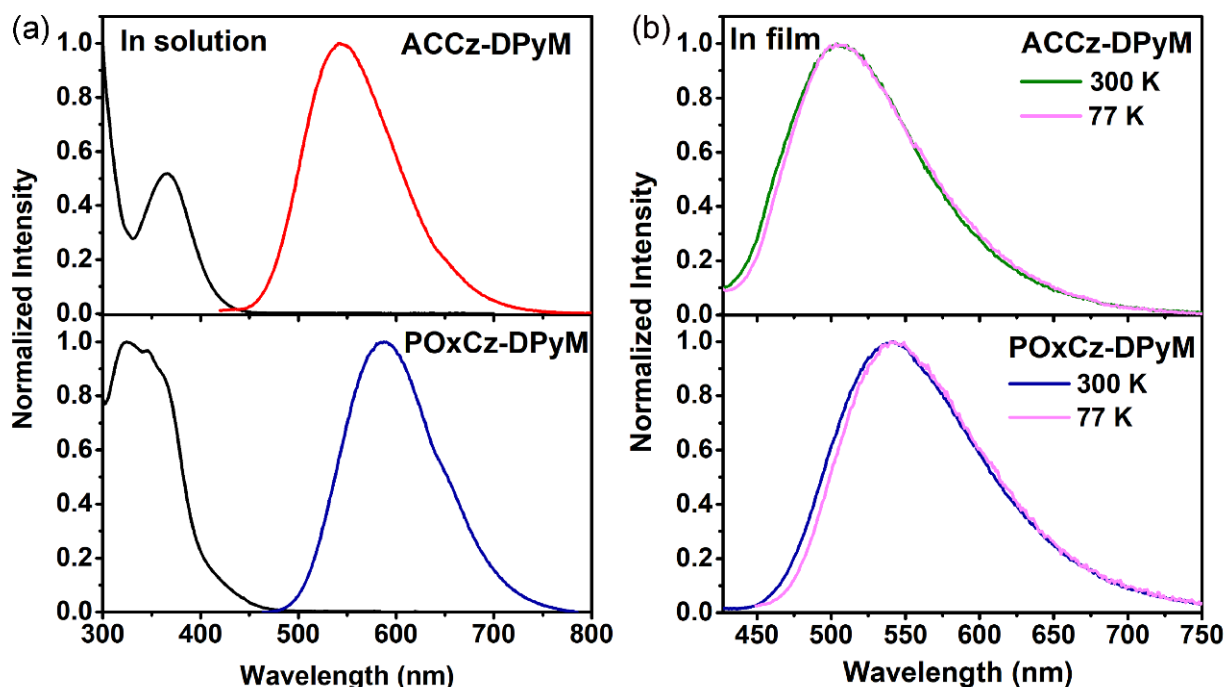


Figure 2. (a) UV spectra and PL spectra in dilute toluene solution for ACCz-DPyM and POxCz-DPyM; (b) PL spectra in film (doped in mCBP with 8 wt%). (λ_{ex} = 360 nm).

Table 1. The test data of ACCz-DPyM and POxCz-DPyM.

Compound	λ_{abs}^a (nm)	$\lambda_{\text{PL}}^a/\lambda_{\text{PL}}^b$ (nm)	$\Phi_{\text{PL}}^b/\%$	$E_{\text{ons}}^{\text{ox}c}$ (V)	HOMO ^d / HOMO ^e (eV)	LUMO ^f / LUMO ^e (eV)	k_{RISC}^g (s ⁻¹)	$\frac{\Delta E_{\text{ST}}^h}{\Delta E_{\text{ST}}^e}$ (eV)	τ_p/τ_d^i [ns]/[μs]	T_d/T_g^j (°C)
ACCz-DPyM	366	541/503	66.2	0.18	-4.98/-4.95	-2.20/-2.45	4.5×10^5	0.04/0.005	39.8/7.2	434/254
POxCz-DPyM	321	590/541	58.2	0.28	-5.08/-4.72	-2.51/-2.53	2.9×10^5	0.04/0.004	98.9/8.7	527/168

^a In solution. ^b Film states. ^c Oxidation potential values. ^d HOMO energy levels deduced from the equation of $\text{HOMO} = -(4.8 + E_{\text{ons}}^{\text{ox}})$. ^e Data of calculations. ^f $\text{LUMO} = \text{HOMO} + E_{\text{opt}}^g$. ^g k_{RISC} : the rate constant for RISC. ^h Subtraction of the onsets of spectra at 300 K and 77 K. ⁱ Obtained in films at 300 K. ^j The heating rate is 10 °C min⁻¹.

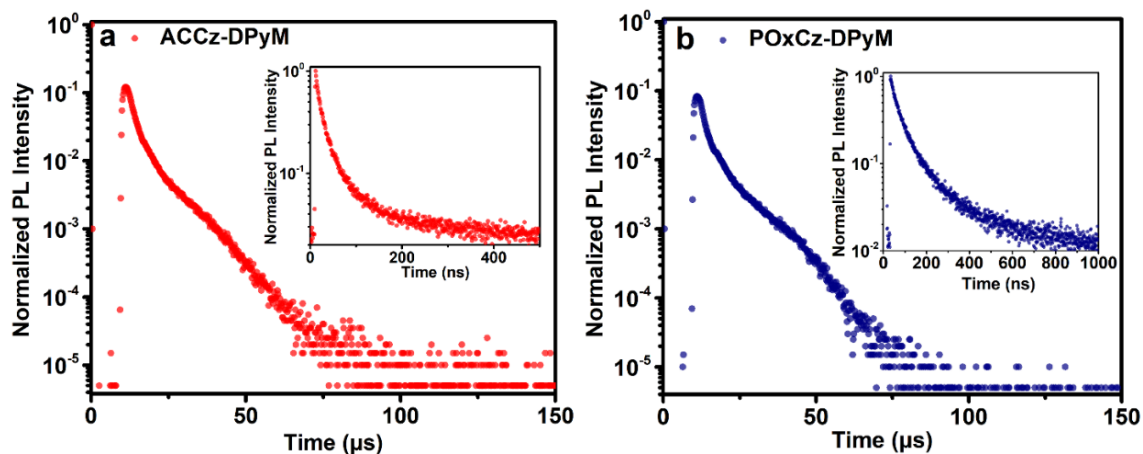


Figure 3. Transient spectra of ACCz-DPyM (a) and POxCz-DPyM (b) in doped films (8 wt% doped in mCBP) at 300 K. Inset: prompt fluorescence.

2.5. Electroluminescence Properties

The solution-processed devices were fabricated to research the electroluminescent characteristics of two emitters ACCz-DPyM and POxCz-DPyM. The devices' structure was the following: ITO/PEDOT:PSS/PVK/mCBP: emitter (8 wt%)/TPBI/Yb/Ag, where PEDOT:PSS and PVK act as the hole-injection and the hole-transporting layer, respectively. TPBI act as the electron-transporting layer. The materials in the emitting layer are ACCz-DPyM and POxCz-DPyM doped in mCBP, respectively. As illustrated in Figure 4d, the electroluminescence spectra of devices come from the luminescence of the emitter without any emission of the host material, which shows that the energy transfer between host and guest materials was completed. Additionally, the devices' electroluminescence spectra show the maximum peaks at 510 and 560 nm with CIE coordinates of (0.28, 0.48) and (0.43, 0.51), respectively. As shown in Figure 4c,d, both solution-processed devices show a good electroluminescence performance. The devices I and II exhibit relatively low driving voltages with 4.0 and 3.4 V, which recorded at a luminance of 1 cd m⁻². The performance of device I shows the L_{max} of 6209 cd m⁻² at 8 V, the CE_{max} of 9.9 cd A⁻¹ and the EQE_{max} of 6.6%. The device II exhibits the performance with L_{max} of 3248 cd m⁻², the CE_{max} of 15.9 cd A⁻¹ and the EQE_{max} of 6.5%, the corresponding data were summarized in Table 2. These results show that both emitters are suitable for solution processing devices. Device I shows a relatively higher electroluminescence performance than that of device II. It could be explained by a better film-forming property of the ACCz-DPyM, which is beneficial to a solution-processed device, and a more molecular rigidity of the ACCz-DPyM than that of POxCz-DPyM, which could suppress the nonradiative transition with higher PLQY [31,33].

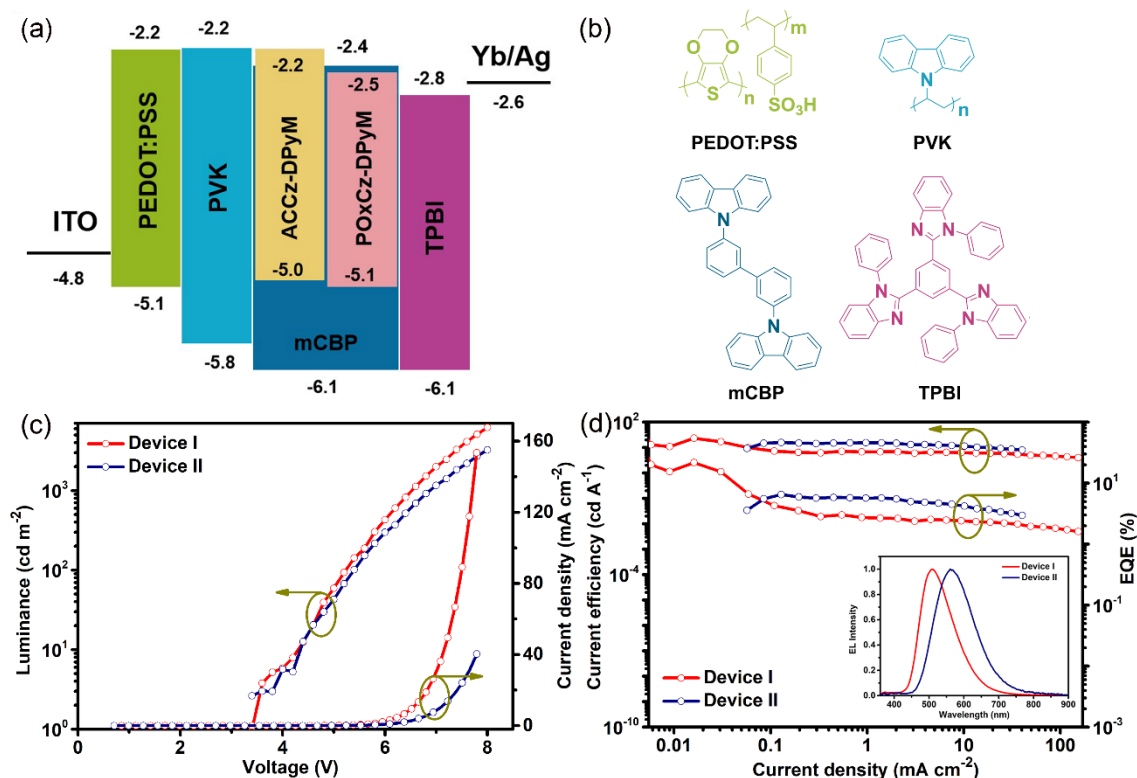


Figure 4. (a) Relative energy level alignments of the materials in the functional layers of the device. (b) Molecular structure of functional layer. (c) The J–V–L characteristics of devices. (d) The CE–J and EQE–J characteristics density of devices. Inset: the EL spectra of devices.

Table 2. The data for electroluminescence performance of devices.

Device	λ_{ELmax} (nm)	V_{on} (V)	L_{max} ($cd\ m^{-2}$)	CE_{max} ($cd\ A^{-1}$)	EQE_{max} (%)	CIE (x, y)
I	510	4.0	6209	9.9	6.6	0.28, 0.48
II	560	3.4	3248	15.9	6.5	0.43, 0.51

3. Conclusions

In conclusion, the ACCz-DPyM and POxCz-DPyM as two novel TADF compounds with ACCz and POxCz as the donor and DPyM as acceptor were synthesized. ACCz-DPyM and POxCz-DPyM have shown high PLQY, small ΔE_{ST} and excellent performances for solution-processed devices. The ACCz-DPyM-based device has shown a higher performance with driving voltages of 4.0 V, the L_{max} of $6209\ cd\ m^{-2}$ at 8 V, the CE_{max} of $9.9\ cd\ A^{-1}$ and the EQE_{max} of 6.6%, which has shown a bluish-green emission. The performance of device II has shown low driving voltages of 3.4 V, L_{max} of $3248\ cd\ m^{-2}$ at 8 V, the CE_{max} of $15.9\ cd\ A^{-1}$, the EQE_{max} of 6.5% and the CIE coordinates of (0.43, 0.51). Additionally, both devices had low efficiency roll-off. Due to the better film-forming properties and more molecular rigidity of ACCz for ACCz-DPyM, the ACCz-DPyM-based solution-processed device has shown better performance than that of POxCz-DPyM.

4. Experimental

4.1. General Information

Unless otherwise stated, all commercially available reactants and solvents were used without further purification. NMR spectra including 1H NMR and ^{13}C NMR spectra were measured on Bruker Avance 400 MHz spectrometer. High-resolution mass spectra were obtained on Bruker Daltonics Inc. (Billerica, MA, USA). UV spectra were measured

with Mapada UV-1800PC (Shanghai, China). PL spectra were collected on Perkinelmer LS-55 (Waltham, MA, USA). The PLQYs of the materials were collected on Edinburgh FLS 980 (Edinburgh, UK). TGA were determined on Hitachi STA7300 (Tokyo, Japan). DSC was measured with Mettler Toledo. CV were performed on CorrTest electrochemical workstation (Wuhan, China). Platinum wire, platinum plate and an Ag/AgNO₃ electrode as the auxiliary electrode, working electrode and quasi-reference electrode were used in CV system. Ferrocenium/ferrocene act as the external standard.

4.1.1. Synthesis of ACCz-DPyM

ACCz of 209 mg (0.36 mmol), DPyM of 60 mg (0.17 mmol), K₃PO₄ of 763 mg (3.6 mmol), CuI of 9.2 mg (0.04 mmol) and 1,2-diaminocyclohexane of 6.0 mg (0.05 mmol) and 1,4-dioxane of 3 mL were added into 20 mL flask. Then, the reaction system was stirred at 110 °C for 12 h under Ar atmosphere. After the reaction was completed, solvent was removed under vacuum; the crude product was purified by column chromatography (hexane: ethyl acetate = 8:1) to obtain ACCz-DPyM. Yield: 50%. ¹H NMR (400 MHz, DMSO) δ 9.35 (d, J = 2.0 Hz, 2H), 8.73 (dd, J = 8.4, 2.4 Hz, 2H), 8.47 (d, J = 1.6 Hz, 4H), 8.42 (d, J = 8.8 Hz, 4H), 8.32 (d, J = 8.8 Hz, 2H), 7.56 (dd, J = 8.8, 1.6 Hz, 4H), 7.50 (dd, J = 7.6, 1.2 Hz, 8H), 6.96 (t, J = 7.6 Hz, 8H), 6.89 (t, J = 7.6 Hz, 8H), 6.27 (d, J = 8.4 Hz, 8H), 1.64 (s, 24H). ¹³C NMR (100 MHz, CDCl₃) δ 190.6, 154.7, 151.6, 141.3, 140.2, 138.8, 135.7, 130.3, 130.1, 129.8, 126.8, 126.3, 125.2, 123.5, 120.6, 118.0, 114.4, 114.1, 36.0, 31.3, 29.7. HRMS (APCI) m/z: [M + H]⁺ calcd for C₉₅H₇₅N₈O⁺, 1343.6058; found, 1343.6081.

4.1.2. Synthesis of POxCz-DPyM

The synthesis method was similar to ACCz-DPyM. The synthesis of POxCz-DPyM using POxCz of 191 mg (0.36 mmol), DPyM of 60 mg (0.17 mmol), K₃PO₄ of 763 mg (3.6 mmol), CuI of 9.2 mg (0.04 mmol), 1,2-diaminocyclohexane of 6.0 mg (0.05 mmol) and 1,4-dioxane of 3 mL. Yield: 48%. ¹H NMR (400 MHz, DMSO) δ 9.30 (d, J = 2.4 Hz, 2H), 8.68 (dd, J = 8.4, 2.4 Hz, 2H), 8.49 (d, J = 2.0 Hz, 4H), 8.36 (d, J = 8.8 Hz, 4H), 8.25 (d, J = 8.4 Hz, 2H), 7.59 (dd, J = 8.8, 2.0 Hz, 4H), 6.76 (dd, J = 7.2, 2.0 Hz, 8H), 6.70–6.61 (m, 16H), 5.95 (dd, J = 7.2, 2.0 Hz, 8H). ¹³C NMR (100 MHz, CDCl₃) δ 190.5, 154.5, 151.5, 144.0, 140.2, 138.9, 129.9, 126.7, 123.2, 121.5, 118.0, 115.4, 114.7, 113.4. HRMS (APCI) m/z: [M + H]⁺ calcd for C₈₃H₅₁N₈O₅⁺, 1239.3977; found, 1239.3994.

4.1.3. Device Fabrication and Measurement

Firstly, the ITO substrate treated with UV-ozone were spin coated with PEDOT:PSS layer (40 nm thick) and heated for 15 min at 150 °C. Then, a PVK interlayer (5 nm) was spin coated on the PEDOT:PSS layer, which annealed for 5 min at 110 °C. Then, the emitters were spin coated on PVK layer with coating speed 2500 rad/min and annealing for 5 min at 100 °C. Moreover, TPBi, Yb and silver cathodes were deposited by evaporation. The performance of OLEDs which contained EQE-L-CE and J-V-L curves were researched by Keithley 2400 (Ohio, USA). The electroluminescence spectra and CIE coordinates were collected on PR-788 photometer (New York State, USA).

Supplementary Materials: The following supporting information can be downloaded at: <https://www.mdpi.com/article/10.3390/photonics10040456/s1>.

Author Contributions: Conceptualization, D.Z., Y.H. and C.Z.; methodology, C.Z.; software, Y.C. and C.Z.; validation, Y.C.; investigation, Y.H., C.Z. and H.Y.; data curation, C.Z. and Y.C.; writing—original draft preparation, Y.H.; writing—review and editing, D.Z., C.Z. and H.Y.; supervision, D.Z.; project administration, D.Z.; funding acquisition, D.Z. All authors have read and agreed to the published version of the manuscript.

Funding: This research was funded by the Natural Science Basic Research Plan in Shaanxi Province of China, grant number 2021JQ-664, In addition, this research was supported by the Scientific Research Program Funded by Shaanxi Provincial Education Department, grant number 19JK0379.

Institutional Review Board Statement: Not applicable.

Informed Consent Statement: Not applicable.

Data Availability Statement: The data are available from the first author and the corresponding author upon reasonable request.

Conflicts of Interest: The authors declare no conflict of interest.

References

1. Uoyama, H.; Goushi, K.; Shizu, K.; Nomura, H.; Adachi, C. Highly efficient organic light-emitting diodes from delayed fluorescence. *Nature* **2012**, *492*, 234–238. [[CrossRef](#)] [[PubMed](#)]
2. Zhang, Q.S.; Li, B.; Huang, S.P.; Nomura, H.; Tanaka, H.; Adachi, C. Efficient blue organic light-emitting diodes employing thermally activated delayed fluorescence. *Nat. Photonics* **2014**, *8*, 326–332. [[CrossRef](#)]
3. Lee, J.; Shizu, K.; Tanaka, H.; Nakanotani, H.; Yasuda, T.; Kaji, H.; Adachi, C. Controlled emission colors and singlet–triplet energy gaps of dihydrophenazine-based thermally activated delayed fluorescence emitters. *J. Mater. Chem. C* **2015**, *3*, 2175–2181. [[CrossRef](#)]
4. Li, B.W.; Li, Z.Y.; Hu, T.P.; Zhang, Y.; Wang, Y.; Yi, Y.P.; Guo, F.Y.; Zhao, L.C. Highly efficient blue organic light-emitting diodes from pyrimidine-based thermally activated delayed fluorescence emitters. *J. Mater. Chem. C* **2018**, *6*, 2351–2359. [[CrossRef](#)]
5. Byeon, S.Y.; Kim, J.; Lee, D.R.; Han, S.H.; Forrest, S.R.; Lee, J.Y. Nearly 100% horizontal dipole orientation and upconversion efficiency in blue thermally activated delayed fluorescent emitters. *Adv. Optical Mater.* **2018**, *6*, 1701340. [[CrossRef](#)]
6. Xiang, S.P.; Lv, X.L.; Sun, S.Q.; Zhang, Q.; Huang, Z.; Guo, R.D.; Gu, H.G.; Liu, S.Y.; Wang, L. To improve the efficiency of thermally activated delayed fluorescence OLEDs by controlling the horizontal orientation through optimizing stereoscopic and linear structures of indolocarbazole isomers. *J. Mater. Chem. C* **2018**, *6*, 5812–5820. [[CrossRef](#)]
7. Li, B.; Yang, Z.; Gong, W.Q.; Chen, X.H.; Bruce, D.W.; Wang, S.Y.; Ma, H.L.; Liu, Y.; Zhu, W.G.; Chi, Z.G.; et al. Intramolecular through-space charge transfer based TADF-active multifunctional emitters for high efficiency solution-processed OLED. *Adv. Optical Mater.* **2021**, *9*, 2100180. [[CrossRef](#)]
8. Zhan, L.S.; Chen, Z.X.; Gong, S.L.; Xiang, Y.P.; Ni, F.; Zeng, X.; Xie, G.H.; Yang, C.L. A simple organic molecule realizing simultaneous TADF, RTP, AIE, and mechanoluminescence: Understanding the mechanism behind the multifunctional emitter. *Angew. Chem. Int. Ed.* **2019**, *58*, 17651–17655. [[CrossRef](#)] [[PubMed](#)]
9. Chan, C.Y.; Cui, L.S.; Kim, J.U.; Nakanotani, H.; Adachi, C. Rational molecular design for deep-blue thermally activated delayed fluorescence emitters. *Adv. Funct. Mater.* **2018**, *28*, 1706023. [[CrossRef](#)]
10. Hirata, S.; Sakai, Y.; Masui, K.; Tanaka, H.; Lee, S.Y.; Nomura, H.; Nakamura, N.; Yasumatsu, M.; Nakanotani, H.; Zhang, Q.S.; et al. Highly efficient blue electroluminescence based on thermally activated delayed fluorescence. *Nat. Mater.* **2015**, *14*, 330–336. [[CrossRef](#)]
11. Lee, Y.H.; Park, S.; Oh, J.; Woo, S.J.; Kumar, A.; Kim, J.J.; Jung, J.; Yoo, S.; Lee, M.H. High-efficiency sky blue to ultradeep blue thermally activated delayed fluorescent diodes based on ortho-carbazole-appended triarylboron emitters: Above 32% external quantum efficiency in blue devices. *Adv. Optical Mater.* **2018**, *6*, 1800385. [[CrossRef](#)]
12. Kim, D.H.; D'Aléo, A.; Chen, X.K.; Sandanayaka, A.D.S.; Yao, D.D.; Zhao, L.; Komino, T.; Zaborova, E.; Canard, G.; Tsuchiya, Y.; et al. High-efficiency electroluminescence and amplified spontaneous emission from a thermally activated delayed fluorescent near-infrared emitter. *Nat. Photon.* **2018**, *12*, 98–104. [[CrossRef](#)]
13. Chan, C.Y.; Tanaka, M.; Nakanotani, H.; Adachi, C. Efficient and stable sky-blue delayed fluorescence organic light-emitting diodes with CIE below 0.4. *Nat. Commun.* **2018**, *9*, 5036. [[CrossRef](#)] [[PubMed](#)]
14. Zhang, Q.S.; Li, J.; Shizu, K.; Huang, S.P.; Hirata, S.; Miyazaki, H.; Adachi, C. Design of efficient thermally activated delayed fluorescence materials for pure blue organic light emitting diodes. *J. Am. Chem. Soc.* **2012**, *134*, 14706–14709. [[CrossRef](#)]
15. Li, C.S.; Ren, Z.J.; Sun, X.L.; Li, H.H.; Yan, S.K. Deep-blue thermally activated delayed fluorescence polymers for nondoped solution-processed organic light-emitting diodes. *Macromolecules* **2019**, *52*, 2296–2303. [[CrossRef](#)]
16. Li, C.S.; Harrison, A.K.; Liu, Y.C.; Zhao, Z.N.; Zeng, C.; Dias, F.B.; Ren, Z.J.; Yan, S.; Bryce, M.R. Asymmetrical-dendronized TADF emitters for efficient non-doped solution-processed OLEDs by eliminating degenerate excited states and creating solely thermal equilibrium routes. *Angew. Chem. Int. Ed.* **2022**, *61*, e202115140.
17. Li, C.S.; Xu, Y.W.; Liu, Y.C.; Ren, Z.J.; Ma, Y.G.; Yan, S.K. Highly efficient white-emitting thermally activated delayed fluorescence polymers: Synthesis, non-doped white OLEDs and electroluminescent mechanism. *Nano Energy* **2019**, *65*, 104057. [[CrossRef](#)]
18. Shi, Y.Z.; Wu, H.; Wang, K.; Yu, J.; Ou, X.M.; Zhang, X.H. Recent progress in thermally activated delayed fluorescence emitters for nondoped organic light-emitting diodes. *Chem. Sci.* **2022**, *13*, 3625–3651. [[CrossRef](#)] [[PubMed](#)]
19. Li, C.S.; Harrison, A.K.; Liu, Y.C.; Zhao, Z.N.; Dias, F.B.; Zeng, C.; Yan, S.K.; Bryce, M.R.; Ren, Z.J. TADF dendronized polymer with vibrationally enhanced direct spin-flip between charge-transfer states for efficient non-doped solution-processed OLEDs. *Chem. Eng. J.* **2022**, *435*, 134924. [[CrossRef](#)]
20. Sun, D.M.; Duda, E.; Fan, X.C.; Saxena, R.; Zhang, M.; Bagnich, S.; Zhang, X.H.; Köhler, A.; Zysman-Colman, E. Thermally activated delayed fluorescent dendrimers that underpin high-efficiency host-free solution-processed organic light-emitting diodes. *Adv. Mater.* **2022**, *34*, 2110344. [[CrossRef](#)]

21. Sun, D.M.; Saxena, R.; Fan, X.C.; Athanasopoulos, S.; Duda, E.; Zhang, M.; Bagnich, S.; Zhang, X.H.; Zysman-Colman, E.; Köhler, A. Regiochemistry of Donor Dendrons Controls the Performance of Thermally Activated Delayed Fluorescence Dendrimer Emitters for High Efficiency Solution-Processed Organic Light-Emitting Diodes. *Adv. Sci.* **2022**, *9*, 2201470. [[CrossRef](#)]
22. Pathak, S.K.; Liu, H.; Zhou, C.J.; Xie, G.H.; Yang, C.L. Triazatruxene based star-shaped thermally activated delayed fluorescence emitters: Modulating the performance of solution-processed non-doped OLEDs via side-group engineering. *J. Mater. Chem. C* **2021**, *9*, 7363–7373. [[CrossRef](#)]
23. Park, I.S.; Komiyama, H.; Yasuda, T. Pyrimidine-based twisted donor–acceptor delayed fluorescence molecules: A new universal platform for highly efficient blue electroluminescence. *Chem. Sci.* **2017**, *8*, 953–960. [[CrossRef](#)] [[PubMed](#)]
24. Huang, R.J.; Kukhta, N.A.; Ward, J.S.; Danos, A.; Batsanov, A.S.; Bryce, M.R.; Dias, F.B. Balancing charge-transfer strength and triplet states for deep-blue thermally activated delayed fluorescence with an unconventional electron rich dibenzothiophene acceptor. *J. Mater. Chem. C* **2019**, *7*, 13224–13234. [[CrossRef](#)]
25. Lee, K.H.; Jeon, S.O.; Chung, Y.S.; Numata, M.; Lee, H.; Lee, E.K.; Kwon, E.S.; Sim, M.; Choi, H.; Lee, J.Y. An excited state managing molecular design platform of blue thermally activated delayed fluorescence emitters by p-linker engineering. *J. Mater. Chem. C* **2020**, *8*, 1736–1745. [[CrossRef](#)]
26. Zeng, X.; Pan, K.C.; Lee, W.K.; Gong, S.L.; Ni, F.; Xiao, X.; Zeng, W.X.; Xiang, Y.P.; Zhan, L.S.; Zhang, Y.; et al. High-efficiency pure blue thermally activated delayed fluorescence emitters with a preferentially horizontal emitting dipole orientation via a spiro-linked double D–A molecular architecture. *J. Mater. Chem. C* **2019**, *7*, 10851–10859. [[CrossRef](#)]
27. Rajamalli, P.; Senthikumar, N.; Huang, P.Y.; Wu, C.C.R.; Lin, H.W.; Cheng, C.H. New molecular design concurrently providing superior pure blue, thermally activated delayed fluorescence and optical out-coupling efficiencies. *J. Am. Chem. Soc.* **2017**, *139*, 10948–10951. [[CrossRef](#)] [[PubMed](#)]
28. Cui, L.S.; Nomura, H.; Geng, Y.; Kim, J.U.; Nakanotani, H.; Adachi, C. Controlling singlet-triplet energy splitting for deep-blue thermally activated delayed fluorescence emitters. *Angew. Chem. Int. Ed.* **2017**, *56*, 1571–1575. [[CrossRef](#)]
29. Luo, J.J.; Gong, S.L.; Gu, Y.; Chen, T.H.; Li, Y.F.; Zhong, C.; Xie, G.H.; Yang, C.L. Multi-carbazole encapsulation as a simple strategy for the construction of solution-processed, non-doped thermally activated delayed fluorescence emitters. *J. Mater. Chem. C* **2016**, *4*, 2442–2446. [[CrossRef](#)]
30. Li, Y.F.; Xie, G.H.; Gong, S.L.; Wu, K.L.; Yang, C.L. Dendronized delayed fluorescence emitters for non-doped, solution-processed organic light-emitting diodes with high efficiency and low efficiency roll-off simultaneously: Two parallel emissive channels. *Chem. Sci.* **2016**, *7*, 5441–5447. [[CrossRef](#)]
31. Huang, B.; Ban, X.X.; Sun, K.Y.; Ma, Z.M.; Mei, Y.N.; Jiang, W.; Lin, B.P.; Sun, Y.M. Thermally activated delayed fluorescence materials based on benzophenone derivative as emitter for efficient solution-processed non-doped green OLED. *Dyes Pigm.* **2016**, *133*, 380–386. [[CrossRef](#)]
32. Wong, M.Y.; Zysman-Colman, E. Purely organic thermally activated delayed fluorescence materials for organic light-emitting diodes. *Adv. Mater.* **2017**, *29*, 1605444. [[CrossRef](#)]
33. Matsuoka, K.; Albrecht, K.; Nakayama, A.; Yamamoto, K.; Fujita, K. Highly efficient thermally activated delayed fluorescence organic light-emitting diodes with fully solution-processed organic multilayered architecture: Impact of terminal substitution on carbazole-benzophenone dendrimer and interfacial engineering. *ACS Appl. Mater. Interfaces* **2018**, *10*, 33343–33352. [[CrossRef](#)]
34. Gong, S.L.; Luo, J.J.; Wang, Z.; Li, Y.F.; Chen, T.H.; Xie, G.H.; Yang, C.L. Tuning emissive characteristics and singlet-triplet energy splitting of fluorescent emitters by encapsulation group modification: Yellow TADF emitter for solution-processed OLEDs with high luminance and ultraslow efficiency roll-off. *Dyes Pigm.* **2017**, *139*, 593–600. [[CrossRef](#)]
35. Rajamalli, P.; Chen, D.Y.; Li, W.B.; Samuel, I.D.W.; Cordes, D.B.; Slawin, A.M.Z.; Zysman-Colman, E. Enhanced thermally activated delayed fluorescence through bridge modification in sulfone-based emitters employed in deep blue organic light-emitting diodes. *J. Mater. Chem. C* **2019**, *7*, 6664–6671. [[CrossRef](#)]

Disclaimer/Publisher’s Note: The statements, opinions and data contained in all publications are solely those of the individual author(s) and contributor(s) and not of MDPI and/or the editor(s). MDPI and/or the editor(s) disclaim responsibility for any injury to people or property resulting from any ideas, methods, instructions or products referred to in the content.